Supplement of Biogeosciences, 12, 7025–7046, 2015
http://www.biogeosciences.net/12/7025/2015/
doi:10.5194/bg-12-7025-2015-supplement

Biogeosciences Open Access EGU

Supplement of

New insights into the organic carbon export in the Mediterranean Sea from 3-D modeling

A. Guyennon et al.

Correspondence to: M. Baklouti (melika.baklouti@mio.osupytheas.fr)

S1 Model Skill Assessment

Due to the high complexity of the biogeochemical model and the scarcity of data, the assessment of the model's representativeness at the scale of the Mediterranean Sea is a complex task. This work, however, aims to achieve comparisons on several modeled variables, at different time and space scales when in situ measurements were available. For reasons of brevity, model outputs hereafter have the prefix "m" while corresponding in situ or satellite observations have the prefix "o".

S1.1 Nutrients

S1.1.1 Basin scale spatial variability

Data collected during the BOUM cruise offer a basis for assessing the quality of the simulation during the stratified summer period. The comparison between mNO_3 and mPO_4 with the corresponding measured concentrations (i.e. oNO3 and oPO4) along the BOUM transect is shown in Fig. S1 and Table S1.

When compared to in situ data, mean mNO_3 [mPO_4 in brackets] in the deep layers (> 1500 m) is underestimated by 1.2 [0.04] μmol l^{-1} in the western basin, and 0.4 [0.01] μmol l^{-1} in the eastern basin. This can be attributed to an underestimation of initial nutrient stocks at depth. There are indeed significant differences between the nutrient concentrations (especially nitrate in the western basin) in deep waters provided by the SeaDataNet climatology data and by the BOUM measurements. As a consequence, and due to the stability of nutrient concentrations in deep water during the simulation, the same disparities can be observed between the model outputs and the BOUM cruise data.

In the surface layer (0-30 m), mNO_3 is less than 1 μmol l^{-1}, with a mean value of around 0.5 μmol l^{-1} for the whole basin, while mPO_4 is almost nil everywhere (< 0.01 μmol l^{-1}). These values are consistent with measured nutrient concentrations, which are low and close to their quantification limits of 0.05 μmol l^{-1} for both NO_3 and PO_4 (Fig. S1, Table S1) though the model tends to overestimate surface nitrate concentrations during periods of intense stratification. This may be related to an overestimation of nitrification processes, and/or an underestimation of detrital organic matter sinking. Nitrification is, indeed, a linear function with a fixed parameter and does not take into account the potential dependence of the process (e.g. Paulmier et al., 2009).

In the western basin, the top of the modeled nitracline is almost 25 m above the top nitracline derived from in situ data, and the gap increases eastward as the top nitracline derived from data gets deeper (Moutin and Prieur, 2012b). The modeled top phosphacline is slightly below the data-derived top phosphacline along most of the BOUM transect. The difference between model outputs and data can also be found in the slope of the nitracline at depths between 150 m and 1000 m: this slope decreases with depth for the model, while it is quite constant for data. As a consequence, significant differences in nitrate concentration can be observed in the "intermediate" waters (between 250 and 1000 m) : mNO3 is underestimated by almost 3 μmol l^{-1} at 500 m in the western basin, and respectively 1.5 and 1.2 μmol l^{-1} in the Ionian and Levantine basins. In the western basin, the same differences between model and data were found in the phosphate vertical profiles (Fig. S1, Table S1), resulting in a maximum difference of 0.15 μmol l^{-1} in phosphate concentrations. However, in the eastern basin, modeled and in situ phosphate gradients are in better agreement than nitrate gradients, except that the phosphacline is less thick than in the data. Finally, some discrepancies between model and observations are attributable to the mislocation of the anti-cyclonic eddies, but this failure of the hydrodynamic model has only a local impact on modeled nutrients.

S1.1.2 Seasonal and vertical variation

The surface patterns of change in mNO_3 and mPO_4 at the DyFaMed station are plotted in Fig. S2. mNO_3 and mPO_4 exhibit a seasonal pattern, with values regularly lower than 0.5 μmol l^{-1} from May (March for mPO_4) to October, increasing thereafter to reach a maximum in January ranging from 3.2 to 4.2 (0.03 to 0.07 for mPO_4) μmol l^{-1} depending on the year. This is very similar to the change in

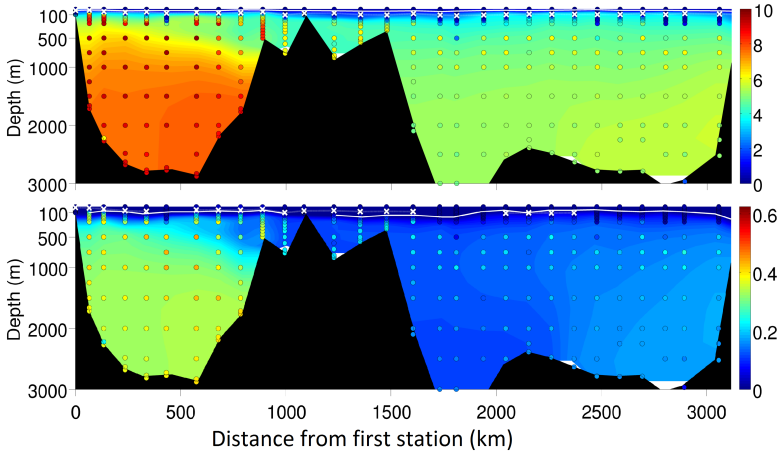

Figure S1. BOUM (top) NO_3 and (bottom) PO_4 (Pujo-Pay et al., 2011). Model outputs are in shaded colors; in situ data are colored circles. Model outputs correspond to the daily outputs averaged over the BOUM cruise period. White crosses represent the data-derived depth of the top nitracline as defined in (Moutin and Prieur, 2012b). The white line indicates the top nitracline from model outputs.

Table S1. Mean over the BOUM cruise period of modeled (mNO_3, mPO_4) and measured (oNO_3, oPO_4) nutrients concentrations for different layers of the western and eastern basins. Root Mean Squared Difference (RMSD) between model outputs and observations have been calculated. Values in brackets are standard deviations, and BQL stands for Below the Quantification Limit (0.05 μmol l^{-1}).

		Model		Observations		RMSD	
		West	East	West	East	West	East
0-30 m	NO_3	0.4 [0.2]	0.6 [0.1]	BQL	BQL	0.44	0.67
	PO_4	0.02 [0]	0.002 [0]	BQL	BQL	0.020	0.0047
250-1500 m	NO_3	6.3 [1]	4.7 [0.4]	8.7 [1.1]	5.3 [1.4]	2.3	1.90
	PO_4	0.27 [0.1]	0.14 [0]	0.37 [0.1]	0.18 [0.1]	0.12	0.047
$>$ 1500 m	NO_3	7.7 [0.1]	5.4 [0.2]	8.9 [0.5]	5.0 [0.5]	1.2	0.33
	PO_4	0.34 [0]	0.15 [0]	0.38 [0]	0.16 [0]	0.049	0.032
Range	NO_3	[0 ; 7.8]	[0.36 ; 5.7]	[BQL ; 9.8]	[BQL ; 6.3]	2.1	1.7
	PO_4	[0 ; 0.34]	[0 ; 0.18]	[BQL ; 0.44]	[BQL ; 0.28]	0.11	0.042

observed NO_3 which is also below 0.5 μmol l^{-1} from May to October and reaches a maximum ranging from 2 to 6.4 μmol l^{-1} in January-February. In summer, however, oNO_3 is often almost below the quantification limit while mNO_3 is never below 0.2 μmol l^{-1}. oPO_4 is below the quantification limit in almost every observation made above 30 m depth, except between January and March where oPO_4 can reach 0.15 μmol l^{-1}. These maxima are underestimated by the model, as mPO_4 never exceeds 0.07 μmol l^{-1} (close to the quantification limit). The differences between mPO_4 and oPO_4 at very low phosphate concentrations can be partly attributable to the lower reliability of measurements near the detection limit. For higher phosphate concentrations however, especially during the winter convection period, there is a clear deficit in the mPO4 which is not only due to the underestimated initial mPO4 concentration in deep waters (this has already been evidenced by the comparison with BOUM data, see Sect. S1.1.1), but also potentially due to an underestimation of the MLD in winter.

Between 30 and 1000 m depth, observed and modeled NO_3 and PO_4 concentrations are consistent with each other though observations show higher mean values and larger ranges quite systematically (see Fig. S3 and S4 and table S2). The highest absolute differences within the water column are observed between 250 and 500 m depth for nitrate where mNO_3 is underestimated by 1.5 μmol l^{-1}, and between 30 and 100 m for phosphate where the mean mPO_4 is very low ($<$ 0.02 μmol l^{-1})

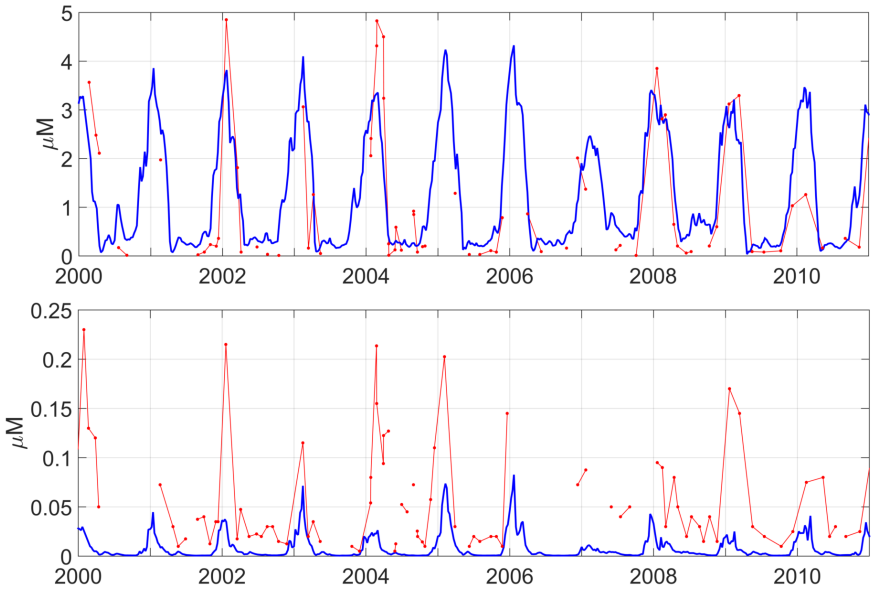

Figure S2. Patterns of change over time of modeled (lines) and observed (dots) surface concentrations in nitrate and phosphate in μmol l^{-1} at the DyFaMed site.

while oPO_4 equals 0.14 μmol l^{-1}. The same interpretation of this poor representation of the shape of the nutriclines (well marked in observations and much more diffuse in the model outputs) as the one provided for the comparison with BOUM profiles can be put forward to explain this model failure, namely underestimated deep nutrient concentrations and a lack of detrital particles that would have reached such water depths before being hydrolyzed. It must be borne in mind, however, that DyFaMed observations are compared to a single grid point of the modeled domain which is submitted to variability due to hydrodynamic features. We evaluated the potential impact of variability by calculating the spatial standard deviation using the 8 neighbouring grid points. The impact of spatial variability is weak on temporal means and stays below 0.5 and 0.04 μmol l^{-1} for NO_3 and PO_4 respectively during the whole period, and therefore cannot fully explain the differences observed.

S1.2 Chlorophyll

S1.2.1 Basin scale variability

Maps of the annual means of oCHL and mCHL as well as their difference (i.e. oCHL-mCHL) over the 2002-2011 period are plotted in Fig. S5 . mCHL is calculated as the average concentration through the first 10 m of the water column.

At first, year-long high chlorophyll clusters can be seen in both oCHL and mCHL close to the main river mouths (the Nile, Rhone, Po, Ebro or Tiber), but only in oCHL in the Dardanelles Strait, along the western coast of the Adriatic Sea and in the Gulf of Gabes. For the Dardanelles Strait, the difference is likely due to a poor representation of the nutrients inputs at this boundary. For the Adriatic Sea, nutrient inputs from rivers are included in the model, but not the ones inferred by anthropic activities (domestic, industrial, agriculture), which may result in an underestimation of the nutrient inputs in this region, and therefore in an underestimation of the chlorophyll concentrations. Finally, the differences between mCHL and oCHL in the Gulf of Gabes is likely due to two main features: first, this region is very shallow, which may produce less reliable satellite data. More importantly, the region of Gabes is characterized by an important industrial production of phosphate which efflu-

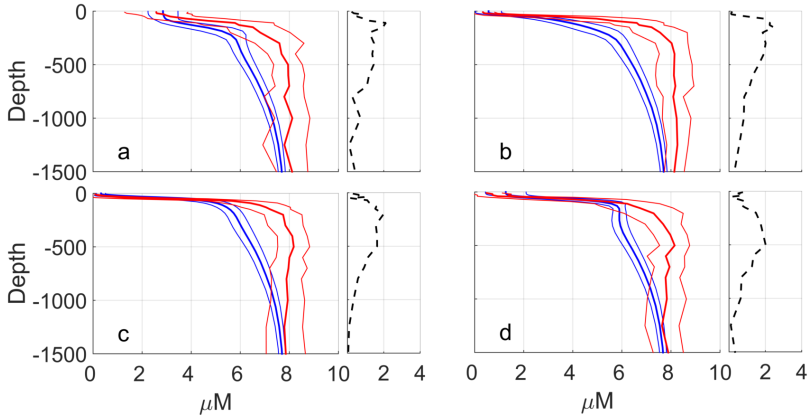

Figure S3. Seasonal climatological data over the 2000-2011 period of modeled (blue lines) and observed (red lines) concentrations in nitrate (μmol l^{-1}) at the DyFaMed site. (a) winter (Dec.-Feb.); (b) spring (Mar.-May); (c) summer (Jun.-Aug.); (d) autumn (Sept.-Nov.). Dotted lines on right panels represent the mean absolute bias between model and data.

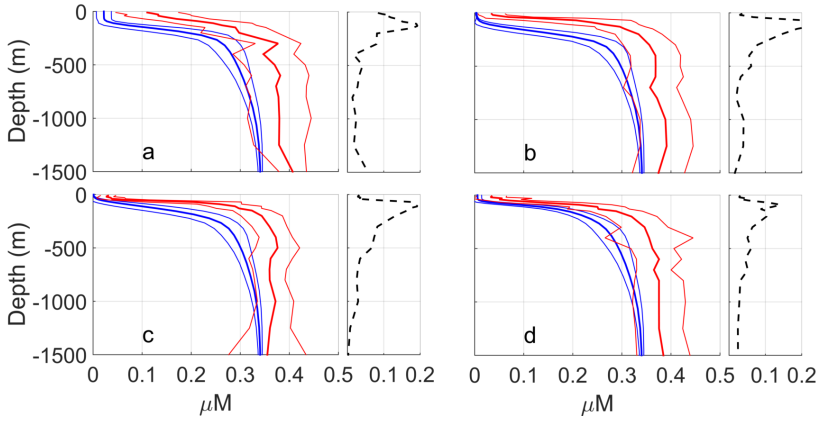

Figure S4. Seasonal climatologies of modeled (blue lines) and observed (red lines) concentrations in phosphate (μmol l^{-1}) at the DyFaMed site. (a) winter (Dec.-Feb.); (b) spring (Mar.-May); (c) summer (Jun.-Aug.); (d) autumn (Sept.-Nov.). Dotted lines on right panels represent the mean absolute bias between model and data.

ents induce a strong enrichment in phosphate in this region, and this is not included in the model. Apart from these permanent features, the main differences between the model and satellite data are observed in the deep convection region of the Liguro-Provencal sub-basin (and extending up to the Ligurian Sea), along the Algerian coast, in the Alboran Sea, and in the south of the eastern basin. The three former are mostly attributable to failures of the hydrodynamic model: first, the fact that the contours of the modeled deep convection region are not the same as the measured ones have already been identified in the hydrodynamical simulation (Beuvier, 2011). Moreover, differences between measured and modeled MLD can also explain differences in the annual surface chlorophyll pattern as for example in the Ligurian Sea where an underestimation of the maximum mNO3 and mPO4 values, likely due to a deficit in the inputs of nutrients from deep waters during winter convection have been evidenced at DyFaMed station (see Fig. S2). The same is true for the Algerian current which is underestimated by the physical model (Soto-Navarro et al., 2014). As a consequence, when the Atlantic waters arrive north of Algeria and Tunisia, they are more nutrient-depleted (and there-

Table S2. Mean over the 2000-2011 period of modeled (mNO_3, mPO_4) and measured (oNO_3, oPO_4) nutrients concentrations at the DyFaMed site for different layers. Root Mean Squared Difference (RMSD) between model outputs and observations have been calculated. Std stands for standart deviation. Spatial variability around the DyFaMed grid point is also assessed through the spatial standart deviation calculated using the 8 neighbour points (first column), and the value given in the table (first column) is the highest deviation calculated during the 2000-2011 period.

			NO_3			
	Spatial Std	mNO_3 mean [range]	mNO_3 Std	oNO_3 mean [range]	oNO_3 Std	RMSD
0-30	0.22	1.3 [0.04-4.3]	1.1	1.0 [BQL-5.2]	1.4	1.1
30-100	0.32	3.0 [0.09 6.1]	1.3	3.8 [BQL-8.3]	2.2	1.8
100-250	0.25	5.1 [1.7-6.7]	1.0	7.0 [2.7-9.6]	1.4	1.4
250-500	0.13	6.2 [5.2-7.2]	0.39	8.1 [5.0-9.9]	0.8	2.0
1000-2000	0.03	7.6 [7.0-7.9]	0.21	8.0 [5.9-9.4]	0.75	0.81
			PO_4			
	Spatial Std	mPO_4 mean [range]	mPO_4 Std	oPO_4 mean [range]	oPO_4 Std	RMSD
0-30	0.001	0.008 [0-0.08]	0.12	1.0 [BQL-0.26]	0.06	0.07
30-100	0.02	0.02 [0-0.19]	0.03	0.14 [BQL-0.54]	0.10	0.16
100-250	0.03	0.15 [0.02-0.33]	0.09	0.29 [0.07-0.45]	0.07	0.17
250-500	0.001	0.29 [0.19-0.33]	0.03	0.35 [0.01-0.46]	0.05	0.08
1000-2000	0.001	0.34 [0.32-0.35]	0.01	0.37 [0.21-0.52]	0.05	0.05

fore less productive) than what is observed. Furthermore, the Atlantic waters that flow along the coast are less dense and therefore strongly isolated from the rest of the water column and it seems that this property is excessively pronounced in the physical model (Beuvier, 2011). As a result, their nutrients content will be too rapidly consumed leading to underestimated primary production and Chl concentrations in this region. Finally, in the Alboran Sea, the high mesoscale activity is probably not fully captured by the hydrodynamic model. In the eastern basin, mCHL is overestimated nearly everywhere, and mostly in the southern part. This difference is however very weak (less than 0.05 μg l^{-1}) and does not clearly appear in the climatological data presented in Fig. S6. Overall, and apart from the hot spots already discussed, the maximum absolute error does not exceed 0.25 μg l^{-1} in the chlorophyll-rich regions of the western basin (i.e. the deep convection region and the core of the eddies in the Alboran Sea) and 0.15(0.05) μg l^{-1} elsewhere in the western (eastern) basin.

In conclusion, though the aforementioned discrepancies between mCHL and oCHL, the model is able to track the location of: i) most of the major productive areas (except the missing regions for which an explanation has already been put forward, ii) a well-marked Liguro-Provencal bloom, which is, nevertheless, more intensive and more extensive in the model, iii) a clearly visible weakly productive northern current (NC), and iv) a patch with high chlorophyll concentrations in the Rhodes Gyre.

S1.2.2 Seasonal surface variability

To further study the seasonal variability of surface chorophyll, we used (for the satellite and model derived chlorophyll concentrations) the metric ΔChl defined as follows :

$$\Delta Chl = \frac{\max(Chl_{\text{year}})}{\text{median}(Chl_{\text{year}})} \quad (1)$$

Since chlorophyll time distribution does not follow a normal law, this indicator is probably more relevant than the mean and the standard deviation. Moreover, since it is applied to climatological data of chlorophyll outputs, extreme values have already been smoothed. High values of ΔChl can

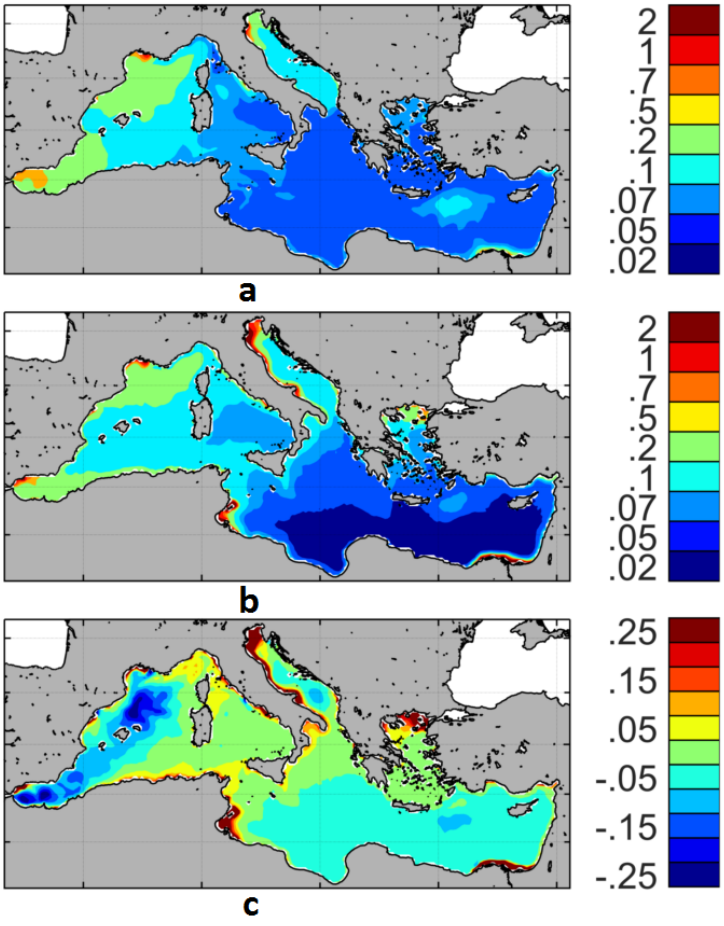

Figure S5. Maps of mean annual surface chlorophyll concentrations (μg l^{-1}) (a) from satellite (i.e. oCHL), (b) from model (i.e. mCHL), and (c) the difference oCHL - mCHL. Model chlorophyll (mCHL) is averaged over the first 10 m of the water column. Period used is 2002-2011 for both model outputs and satellite data.

therefore be related to a strong seasonal variability, while low values, typically < 2, can be associated with a constant signal (Fig. S6).

For both model and satellite, the seasonal signal is particularily strong in the Liguro-Provencal sub-basin ($\Delta Chl > 10$) and the Algerian Coast (ΔChl_{sat} about 8, ΔChl_{mod} above 10). ΔChl is broadly above 6 for the model and 4 for satellite data in the western basin west of 9°W. In the Tyrrhenian Sea, ΔChl is close to zero for the model, except for the area along the Italian Coast, while ΔChl for satellite data, it is above 3, with a maximum value around 6.

In the eastern basin, model ΔChl is almost nil everywhere except in the Rhodes Gyre (> 10) and in the Adriatic Sea where two patches of values above 10 can be seen. oCHL values are also low, except in the south Ionian basin (where $\Delta Chl \approx 2$), the Rhodes Gyre and the Gulf of Gabes ($\Delta Chl > 6$). In the Adriatic sea, a patch of values of ΔChl above 3 is visible in the south.

Using SeaWiFS and MODIS surface chlorophyll data from 1998 to 2010 and statistical work from D'Ortenzio and Ribera d'Alcalà (2009), Lavigne et al. (2013) identified 9 different regions on the basis of the seasonality of the chlorophyll signal. These regions are consistent with those emerging from the present study. The north-west bloom region is associated with the region of the highest values of ΔChl_{mod} and ΔChl_{sat}. The Algerian region is characterized by relatively high ΔChl

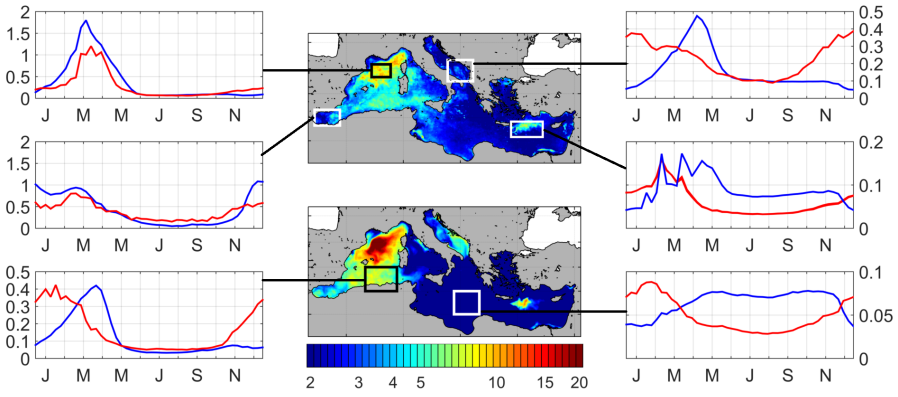

Figure S6. Maps of the ratio ΔChl (Eq. 1) between annual maximum and annual median for satellite (top) and model (bottom) chlorophyll surface concentrations over the 2002-2011 period. A climatology of oCHL (red lines) and mCHL (blue lines) over the same period is also plotted for the most representative regions.

values, while the intermittent Rhodes Gyre region is identified as highly variable in the present study according to satellite data and model outputs. The distinction between the southern and northern Ionian basins in the bioregionalization, also visible satellite ΔChl is however absent in the model ΔChl.

The comparison of modeled and observed time series (climatological data over the 2000-2011 period) provides additional information on the modeli's ability to reproduce surface chlorophyll seasonal variations. Though the model values of the central eastern basin are within the range of observations in the open sea (see Fig. S5), the highest discrepancy in the seasonal signal is observed in the oligotrophic region of the Levantine basin: the mCHL seasonal signal is in phase opposition with that of oCHL, and the maximum mCHL is obtained in summer-autumn against winter for oCHL. Comparison between models is beyond the scope of this paper, however comparisons with former simulations (Lazzari et al., 2012; Mattia et al., 2013) can offer some information. It is noteworthy that results from Mattia et al. (2013) showed a greater bias in the eastern basin than in the western basin, with higher annual concentrations compared to satellite measurements. However, the maximum of surface chlorophyll in the eastern basin was simulated in winter (as for satellite chlorophyll) in Mattia et al. (2013). This is also the case in the simulation run by Lazzari et al. (2012), however summer concentrations seemed to be underestimated in that case. This shortcoming can however be largely relativized by the fact that the mean surface chlorophyll in summer-autumn does not differ significantly from the satellite measurement. Furthermore, surface chlorophyll in the model is estimated as the mean over the first 10 m of the water column, and therefore includes part of the chlorophyll gradient towards the Deep Chlorophyll Maximum (DCM) which is shallower than that observed in the eastern basin during the stratification period (results not shown though the same bias is observed at the DyFaMed site, see Sect. S1.2.3). Finally, the summer functioning of the surface layer is well reproduced by the model : small phytoplankton are largely dominant and maintain their activity because of the microbial loop (Siokou-Frangou et al., 2010).

A shift in chlorophyll maximum can also be seen in the south of the western basin, with an earlier and longer bloom in oCHL than in mCHL. This could be partly due to the aforementioned tendency of the model to exagerate the isolation of the surface Atlantic waters from the rest of the water column, thus delaying the input of nutrients from deep water through winter convection. Finally, in the Adriatic Sea, a delayed input of nutrients from deep waters combined with the presence of two eddies with high core mCHL values in winter and mostly in spring that are not observed on oCHL (the position of the two eddies can be seen on the primary production map in Fig. S8), probably explains the shift between oCHL and mCHL. Conversely, in regions associated with high nutrient

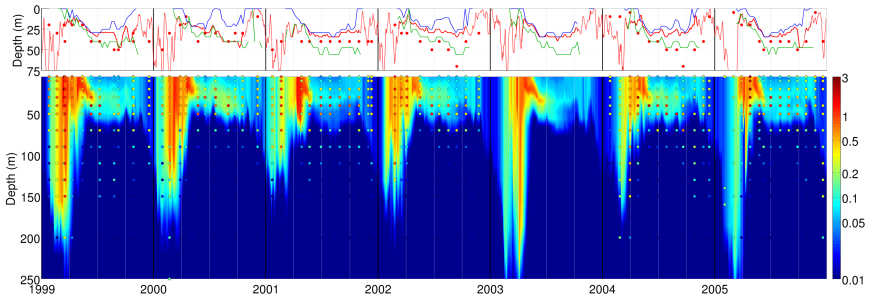

Figure S7. Patterns of change over time of vertical concentrations of chlorophyll (μg l^{-1}) at the DyFaMed site, with model outputs in shaded colors and in situ data (Marty et al., 2008) in colored dots. Top, the depth of chlorophyll maximum is represented with red dots for in situ data and the red line for the model. Depths of maximum chlorophyll for small phytoplankton (blue) and large plankton (green) are also plotted.

inputs (Ligurian Sea, Alboran Sea) the temporal pattern of change of surface chlorophyll is reproduced by the model but concentrations are overestimated during the bloom in the deep convection region, probaly due to too intensive winter mixing (Beuvier, 2011).

S1.2.3 Vertical variability

At the DyFaMed station, strong seasonal variability in chlorophyll concentrations can be observed in both model outputs and in situ data (Marty et al., 2002; Marty and Chiavérini, 2010). Chlorophyll data (oCHL) and modeled data (mCHL) are mutually consistent as shown in Fig. S7: they both show a bloom occurring in late February early March after the period of maximum mixing (mid February in this area), and characterized by high chlorophyll concentrations within the mixing layer (down to 150 m depth). A second less intense and shallower bloom often follows in April, characterized by chlorophyll concentrations above 1.5 μg l^{-1} in both model outputs and observations. During summer, surface concentrations are at their lowest level with values of mChl and oChl often below 0.1 μg l^{-1}, while their maximum values are observed in early spring.

Following April, a DCM is visible in both observations and model, though it is shallower in the model and its intensity decreases more rapidly than in observations (see Fig. S7-top).

However, when looking at the two chlorophyll contributors of the model, it appears that the position of the DCM associated with large phytoplankton is close to that observed. This means that the difference in the DCM depth is probably due to the underestimation of large phytoplankton concentrations at depth by the model during summer, that may be inferred by the already identified underestimation by the model of nutrient stocks in the intermediate layer (see Sect. S1.1.1).

S1.3 Primary production

In the following section, mIPP refers to the modeled integrated Gross Primary Production, i.e. to the total amount of inorganic carbon fixed by the two phytoplankton groups integrated over the water column. The equivalent for observations will be referred to as oIPP.

S1.3.1 Spatial variability

The mean annual mIPP for the whole basin over the 2000-2012 period equals 82 gC m^{-2} y^{-1}, which is within the range of published values (see Table S3). In this table, the studies by Bosc et al. (2004) and Uitz et al. (2012) both show quite similar oIPP spatial distributions despite the two analyses having been conducted during different periods (1997-2001 for Bosc et al. (2004) and 1998-2007 for Uitz et al. (2012)). IPP calculated by Bosc et al. (2004) tend to overestimate observations, particularily in ultra-oligotrophic regions while IPP from Uitz et al. (2012) does not show a trend

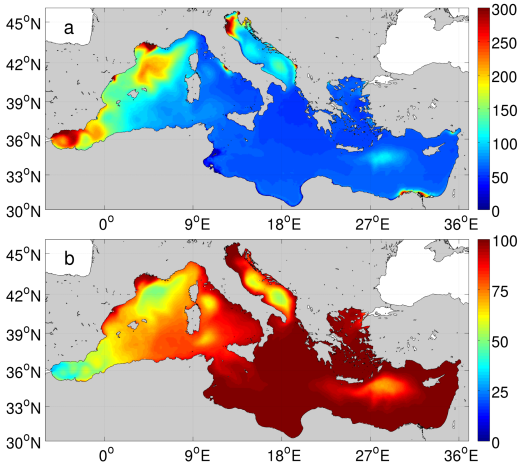

Figure S8. (a) Annual gross primary production calculated over the 2000-2012 period and integrated through the whole water column, in gC m^{-2} y^{-1}, (b) proportion of production due to small phytoplankton group, in % .

of error. In the different geographical regions defined in Bosc et al. (2004) and reported in Tab. S3, mIPP is mostly within the range defined by the two aforementioned studies. More importantly, the hierarchy in terms of IPP values between the different regions is the same for the model and the satellite products.

mIPP values in the Mediterranean Sea range between 35.4 and 270 gC m^{-2} y^{-1}, showing a strong spatial heterogeneity (see Fig. S8a). A gradient in mIPP is observed from west to east : the western basin production is almost twice that of the eastern basin, which is coherent with the dissimilarity in chlorophyll and nutrients already mentioned. This ratio is also coherent with the oIPP values derived from in situ measurements (Moutin and Raimbault, 2002), but higher than that found using satellite data (Uitz et al., 2012; Bosc et al., 2004) or another model (Lazzari et al., 2012).

Figure S8b shows that, except in the regions that benefit from permanent or episodic nutrient inputs from the deep sea (i.e. the deep convection region in the Liguro-Provencal sub-basin, eddies in the Alboran, Adriatic Seas and the Rhodes Gyre region), mIPP is mostly due to small phytoplankton throughout the Mediterranean Basin. In the eastern basin, the proportion of IPP due to small phytoplankton is close to 100% everywhere, except in the Levantine basin in the region of the Rhodes Gyre. These results are consistent with in situ studies (Siokou-Frangou et al., 2010; MERMEX-group, 2011).

S1.3.2 Seasonal variability

In addition to satellite data, in situ oIPP measured at the DyFaMed station between 2002 and 2006 (Marty et al., 2008) were used for comparison with mIPP (Fig. S9). The model and observations show very similar patterns, with a maximum in March-April, and a slight decrease from July to December. The correlation between mIPP and oIPP is significant as suggested by the right panel in Fig. S9, and does not show any bias though the model fails to reproduce the highest oIPP values.

Table S3. Integrated gross primary production (IPP in gC m^{-2} y^{-1}) for the different regions defined by Bosc et al. (2004) and for the whole Mediterranean Basin. mIPP values calculated by the model are compared to IPP values derived from the following references: (a) Bosc et al. (2004), (b) Uitz et al. (2012) (c) Antoine et al. (1995), (d) Lazzari et al. (2012), and (e) Sournia (1973). References (a) to (c) refer to satellite data, (d) to another modeling study, and (e) to a climatology of ^{14}C measurements

Region	Model (mIPP)	(a)	(b)	(c)	(d)	(e)
Alboran Sea	222	150	230			
Gulf of Lion	182	97	194			
Balearic Sea	145	80	167			
Algero-Provencal basin	123	78	153			
Ligurian Sea	109	80	165			
Algerian basin	107	78	163			
Adriatic Sea	102	71	182			
Tyrrhenian Sea	66	67	137			
South Levantine basin	65	59	105			
North Levantine basin	63	60	106			
South Ionian Sea	60	61	115			
North Ionian Sea	55	63	126			
Mediterranean Basin	82	68	136	156	98	80-90

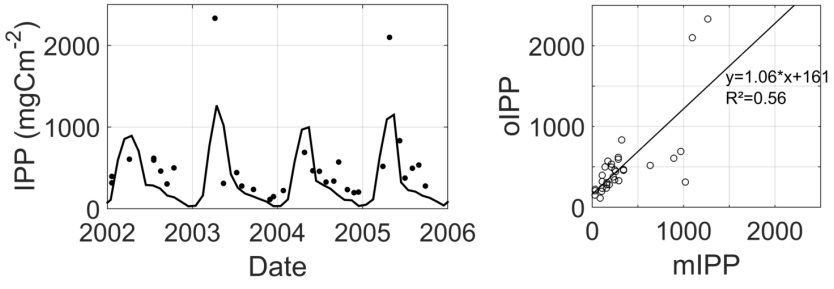

Figure S9. Patterns of change over time of monthly integrated gross primary production (IPP) in mg C^{-2} d^{-1}. oIPP correspond to 0-100 m in situ measurements extracted from the DyFaMed database (dots) and mIPP correspond to the 0-100 m IPP provided by the model during the same period (black line). oIPP were converted to daily gross primary production according to the Moutin et al. (1999) method.

S1.4 Dissolved organic carbon

Regular measurements of total DOC (i.e. including refractory (RDOC) and semi-refractory (SRDOC) pools) performed at the DyFaMed site (Avril, 2002), were used for comparison. Since the model only provides the labile and semi-labile DOC pools, the in situ DOC concentration measured in deep water ($>$ 1000 m), which can be considered as refractory DOC, has been added to the model DOC output. Moreover, since our run does not cover the period of the in situ data, we decided to work on a climatological survey of DOC vertical profiles: bi-monthly mean, maximum and minimum DOC values were calculated and compared (Fig. S10).

At the DyFaMed grid point, mDOC stock is underestimated throughout the whole water column during winter. Then, mDOC and oDOC increase during spring (April-May), but only near the surface for mDOC. In summer, the mDOC and oDOC values remain high in the upper layers, and finally decrease in autumn. If these seasonal variations are well reproduced by the model, high differences can however be seen between mDOC and oDOC. If we first focus on the 0-100 m layer, DOC concentrations and seasonal variations of both the model and observations are at a maximum at the surface, but from spring to autumn, mDOC is higher than oDOC near the surface (roughly in the 0-50 m layer), and lower between 50 and 100 m depth, resulting in higher vertical DOC gradients in the model. The same discrepancy can also be evidenced (mostly in the western basin) from the comparison between mDOC and oDOC during the BOUM cruise that took place in summer (Fig. S11). The overestimated near-surface DOC concentrations may be attributable to an excessive P-limitation in the model near the free surface, probably due to too low phosphate deep concentrations (see also the Discussion section in the Manuscript for the description of the DOC accumulation process under P depletion). The shallower and underestimated DCM as compared to that measured (see Sect. S1.2.3) may also partly explain the discrepancy since photosynthesis rates are underestimated. As a consequence, the excess of newly synthetized carbon through photosynthesis which fuels the DOC pool is probably underestimated in the region of the modeled DCM and even below. Too easy access for bacteria to SLDOC, resulting in overcomsuption of DOC by nutrient-replete bacteria, is another possible explanation of this bias.

mDOC concentrations are systematically lower than those of oDOC beyond 100 m depth. The latter argument relative to SLDOC access by bacteria could also partly explain the systematically underestimated mDOC concentrations below 100 m depth. Again, this model failure is also observed during the BOUM cruise (Fig. S11).

The comparison between oDOC and mDOC requires the addition of an unknown DOC component, namely the semi-refractory and the refractory pools, to the mDOC value. It is indeed generally assumed that both these pools are constant across the water column and that they correspond to the deep DOC concentration (i.e. 40 μM at DyFaMed station), but this is a clear source of bias, especially below 100 m depth where the SRDOC concentrations are significant and may vary, as suggested in Santinelli et al. (2010).

The fact that the modeled 0-100 m integrated stocks are quite similar to the measured ones (though the slight underestimation in the eastern basin during the BOUM cruise since DOC accumulation has not yet reached its maximum value in summer) is however an essential point as regards the DOC export at 100 m.

Finally, the Taylor diagram presented in Fig. S12 summarizes the numerous comparisons between model outputs and the DyFaMed station observations undertaken in the present study.

In conclusion, some critical appraisal concerning the datasets (from DyFaMed station and BOUM cruise) used in this study for the model skill assessment, can also be done. The BOUM cruise took place in summer (June-July 2008) during the stratified period in which nutrient concentrations in the surface layer are very low, and even under the quantification limits in the eastern basin. A rigorous assessment of the nutrient concentrations provided by the model in this layer is therefore impossible. Moreover, the cruise lasted 1.5 months, and the nutrient maps to which model outputs were compared do not correspond to a snapshot but rather to a collection of data gathered at different times. This may partially bias the comparison with model outputs since the latter were averaged over the period

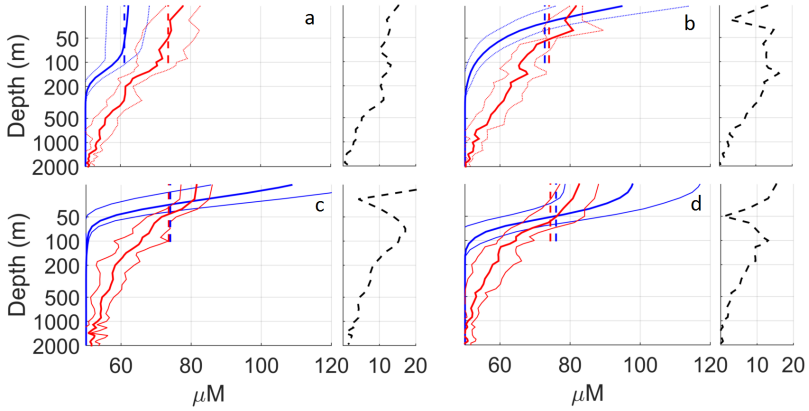

Figure S10. Vertical profiles of total DOC (μmol l^{-1}) at DyFaMed site (a) in winter, (b) spring, (c) summer and (d) autumn. mDOC are weekly averaged outputs. Blue and red lines respectively refer to modeled (mDOC) and measured (oDOC) DOC. Thick lines represent the mean of DOC over the period, while thin lines represent the standard deviation for each depth. oDOC and mDOC respectively cover the 1991-1993 (Avril, 2002) and the 2000-2012 simulation period. The dotted lines in the right panels represent the mean absolute bias between oDOC and mDOC.

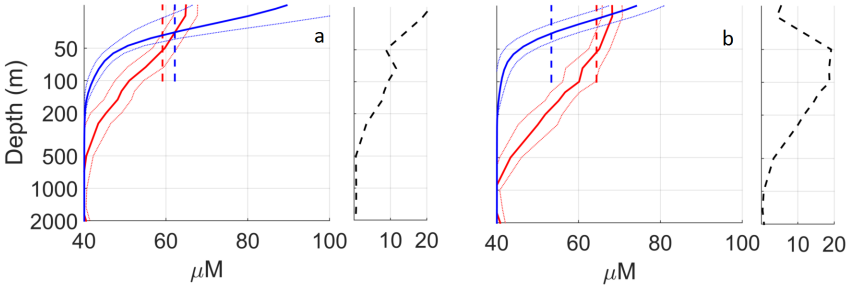

Figure S11. Vertical profiles of total DOC (μmol l^{-1}) during the BOUM cruise. mDOC are weekly averaged outputs over the whole BOUM section. Blue and red lines respectively refer to modeled (mDOC) and measured (oDOC) DOC. Thick lines represent the mean of DOC over the period, while thin lines represent the standard deviation for each depth. The dotted lines in the right panels represent the mean absolute bias between oDOC and mDOC.

of the cruise. Concerning the DyFaMed site, it is affected by many mesoscale processes that are known to generate high variability in data which are not necessarily representative of the trends at sub-basin scale. This may also generate potential bias for the comparison between model outputs and in situ data. Finally, though the aforementioned bias, these datasets are essential, since, except near the coasts, there is a clear lack of datasets including the large variety of data that are necessary to assess a biogeochemical model such as Eco3M-MED.

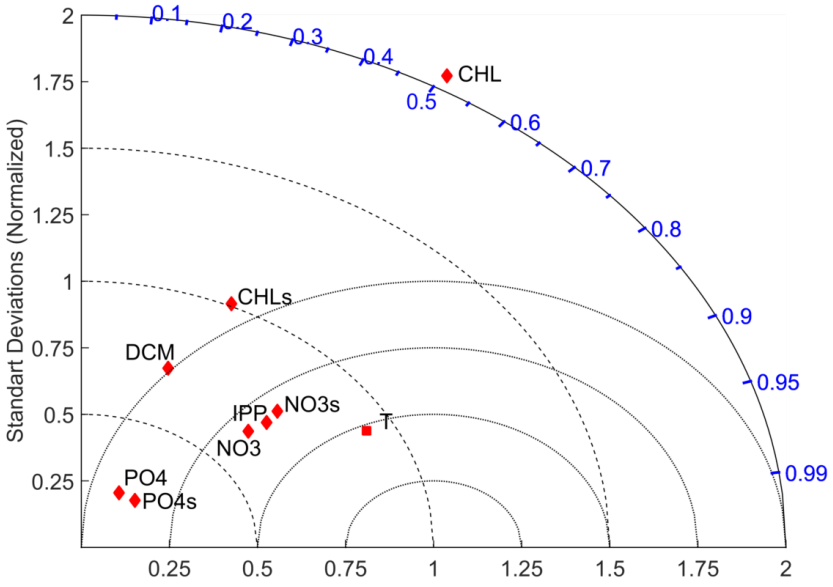

Figure S12. Taylor diagram of simulated and observed variables in the 0-100 m layer. Model outputs and in situ data are taken at the same depth and time. PO4s, NO3s and CHLs are surface concentrations of phosphate, nitrate and chlorophyll respectively. T refers to temperature. Chlorophyll concentrations are log-transformed.

References

Antoine, D., Morel, A., and André, J.: Algal pigment distribution and primary production in the eastern Mediterranean as derived from coastal zone color scanner observations, Journal of Geophysical Research, 100, 16 193–16, 1995.

Avril, B.: DOC dynamics in the northwestern Mediterranean Sea (DYFAMED site), Deep Sea Research Part II: Topical Studies in Oceanography, 49, 2163–2182, 2002.

Beuvier, J.: Modélisation de la variabilité climatique de la circulation et des masses d'eau en mer Méditerranée: impact des échanges océan-atmosphére, Ph.D. thesis, Ecole Polytechnique, 2011.

Bosc, E., Bricaud, A., and Antoine, D.: Seasonal and interannual variability in algal biomass and primary production in the Mediterranean Sea, as derived from 4 years of SeaWiFS observations, Global Biogeochemical Cycles, 18, GB1005, doi:10.1029/2003GB002034, 2004.

D'Ortenzio, F. and Ribera d'Alcalà, M.: On the trophic regimes of the Mediterranean Sea: a satellite analysis, Biogeosciences, 6, 139–148, 2009.

Lavigne, H., D'Ortenzio, F., Migon, C., Claustre, H., Testor, P., d'Alcalà, M., Lavezza, R., Houpert, L., and Prieur, L.: Enhancing the comprehension of mixed layer depth control on the Mediterranean phytoplankton phenology, Journal of Geophysical Research: Oceans, 118, 3416–3430, 2013.

Lazzari, P., Solidoro, C., Ibello, V., Salon, S., Teruzzi, A., Béranger, K., Colella, S., and Crise, A.: Seasonal and inter-annual variability of plankton chlorophyll and primary production in the Mediterranean Sea: a modelling approach, Biogeosciences, 8, 5379–5422, 2012.

Marty, J. and Chiavérini, J.: Hydrological changes in the Ligurian Sea (NW Mediterranean, DYFAMED site) during 1995–2007 and biogeochemical consequences, Biogeosciences, 7, 2117–2128, 2010.

Marty, J., Chiavérini, J., Pizay, M., and Avril, B.: Seasonal and interannual dynamics of nutrients and phytoplankton pigments in the western Mediterranean Sea at the DYFAMED time-series station (1991–1999), Deep Sea Research Part II: Topical Studies in Oceanography, 49, 1965–1985, 2002.

Marty, J.-C., Garcia, N., and Raimbault, P.: Phytoplankton dynamics and primary production under late summer conditions in the NW Mediterranean Sea, Deep Sea Research Part I, 55, 1131–1149, 2008.

Mattia, G., Zavatarelli, M., Vichi, M., and Oddo, P.: The Eastern Mediterranean Sea biogeochemical dynamics in the 1990s: A numerical study, Journal of Geophysical Research: Oceans, 118, 2231–2248, 2013.

MERMEX-group: Marine ecosystems' responses to climatic and anthropogenic forcings in the Mediterranean, Progress in Oceanography, 91, 97–166, 2011.

Moutin, T. and Prieur, L.: Influence of anticyclonic eddies on the Biogeochemistry from the Oligotrophic to the Ultraoligotrophic Mediterranean (BOUM cruise), Biogeosciences, 9, 3827–3855, 2012b.

Moutin, T. and Raimbault, P.: Primary production, carbon export and nutrients availability in Western and Eastern Mediterranean Sea in early summer 1996 (MINOS cruise), Journal of Marine Systems, 33, 273–288, 2002.

Moutin, T., Raimbault, P., and Poggiale, J.: Production primaire dans les eaux de surface de la Mediterranee occidentale. Calcul de la production journaliere, Comptes Rendus de l'Académie des Sciences-Series III-Sciences de la Vie, 322, 651–655, 1999.

Paulmier, A., Kriest, I., and Oschlies, A.: Stoichiometries of remineralisation and denitrification in global biogeochemical ocean models, Biogeosciences (BG), 6, 923–935, 2009.

Pujo-Pay, M., Conan, P., Oriol, L., Cornet-Barthaux, V., Falco, C., Ghiglione, J., Goyet, C., Moutin, T., and Prieur, L.: Integrated survey of elemental stoichiometry (C, N, P) from the western to eastern Mediterranean Sea, Biogeosciences, 8, 883–899, 2011.

Santinelli, C., Nannicini, L., and Seritti, A.: DOC dynamics in the meso and bathypelagic layers of the Mediterranean Sea, Deep Sea Research Part II: Topical Studies in Oceanography, 57, 1446–1459, 2010.

Siokou-Frangou, I., Christaki, U., Mazzocchi, M., Montresor, M., Ribera d'Alcalà, M., Vaqué, D., and Zingone, A.: Plankton in the open Mediterranean Sea: a review, Biogeosciences, 7, 1543–1586, 2010.

Soto-Navarro, J., Somot, S., Sevault, F., Beuvier, J., Criado-Aldeanueva, F., García-Lafuente, J., and Béranger, K.: Evaluation of regional ocean circulation models for the Mediterranean Sea at the Strait of Gibraltar: volume transport and thermohaline properties of the outflow, Climate Dynamics, 44, 1277–1292, doi:10.1007/S00382-014-2179-4, 2014.

Sournia, A.: La production primaire planctonique en Méditerranée; essai de mise à jour, Cooperative Investigations in the Mediterranean, International Coordinator and Operational Unit; Étude en commun de la Méditerranée, Coordonnateur international et Unité opérationnelle, 1973.

Uitz, J., Stramski, D., Gentili, B., D'Ortenzio, F., and Claustre, H.: Estimates of phytoplankton class-specific and total primary production in the Mediterranean Sea from satellite ocean color observations, Global Biogeochemical Cycles, 26, doi:10.1029/2011GB004055, 2012.